CNOP based on ACPW for Identifying Sensitive Regions of Typhoon Target Observations with WRF Model

Bin Mu[1], Linlin Zhang[1], Shijin Yuan[1], Wansuo Duan[2]

5   [1]School of Software Engineering, Tongji University, Shanghai 201804
[2]State Key Laboratory of Numerical Modeling for Atmospheric Sciences and Geophysical Fluid Dynamics, Institute of Atmospheric Physics, Chinese Academy of Sciences，Beijing 100029, China

Correspondence to: Shijin Yuan (yuanshijin2003@163.com)

10

Abstract.

In this paper, we rewrite the ACPW (adaptive cooperation co-evolution of parallel particle swarm optimization and wolf search algorithm based on principal component analysis) and applied it to solve conditional nonlinear optimal perturbation (CNOP) in the WRF-ARW for identifying sensitive areas of typhoon target observations, which is proposed by us in the

15   study of Zhang et al. (2018), to investigate its feasibility and effectiveness in the WRF-ARW model. Fitow (2013) and Matmo (2014) are taken as two typhoon cases, and simulated with the ~~60 km~~60-km horizontal resolution. The total dry energy is adopted as the objective function. The CNOP is also calculated by the method based on the adjoint model (~~ADJ method~~ADJ method) as a benchmark. To evaluate the ACPW-CNOP, five aspects are analysed, such as the pattern, energy, similarity, benefits from the CNOPs reduced in the whole domain and the sensitive regions identified, and the simulated

20   typhoon tracks. The experimental results show that the temperature and wind patterns of ACPW-CNOP is similar to those of the ADJ-CNOP in all typhoons. And the similarity values of ADJ-CNOP and ACPW-CNOP of two typhoon cases are more than 0.5. When reducing CNOPs in the sensitive regions, the forecast ~~income~~benefit of ACPW-CNOP is greater than that of ADJ-CNOP in all typhoons. Moreover, the sensitive regions identified by the ACPW-CNOP has the similar influence with the ADJ-CNOP on the simulation of typhoon tracks, sometimes the ACPW-CNOP has more positive impact on the

25   simulation of typhoon tracks. The ACPW is more efficient than the ~~ADJ method~~ADJ method in this paper.

1 Introduction

Target observation is an effective way to improve the typhoon forecast skills, which is a study of the typhoon predictability (Franklin and Demaria, 1992; Bergot, 1999; Aberson, 2003). Conditional nonlinear optimal perturbation (CNOP) proposed by Mu and Duan (2003) is an effective method for studying the typhoon predictability (Mu and Duan, 2003). And many

30   researchers use CNOP method to identify sensitive areas of typhoon target observations (TTOs). MM5 (The Fifth-Generation Mesoscale Model) model was adopted in the ~~M~~most of ~~the~~ current studies of sensitive areas identification ~~adopt~~

the (Zhou and Mu, 2011; Zhou and Mu, 2012a; Zhou and Mu, 2012b; Zhou and Zhang, 2014). Zhou and Mu (2011) investigated the affection of the different verification regions to the sensitive area identifications, and ~~summary~~summarized that the little shift range and size of the verification regions will not affect the structure of CNOP. Zhou and Mu (2012a) also ~~study~~ studied the affection of different horizontal resolutions and found that the higher resolution ~~will~~ would show the more

5 small-scale information of CNOP. They also research~~ed~~ the different dependency of integration times and regimes (2012b), and the solutions guide~~d~~ the future research. Zhou and Zhang (2014) ~~study~~ studied three sensitive area identification schemes and recommend~~ed~~ the vertically integrated energy scheme~~.~~.

However, the MM5 model is not updated and maintained after 2006. Nowadays, the popular mesoscale model is WRF-ARW (Advanced Research the Weather Research and Forecast) model. Recently, there is only one study which ~~to~~ identify

10 sensitive areas by using the WRF-ARW model (Yu et al., 2017~~Skamarock et al, 2008~~). Yu et al. (2017) use the SPG2 (spectral projection gradient 2 ~~(SPG2)~~ algorithm (Ernesto et al., 2001) to solve CNOP~~,~~. As we all know that ~~T~~the SPG2 algorithm must use the adjoint model to obtain the gradient information for updating the search direction. ~~but~~ But the adjoint model of WRF-ARW only has one gravity dragging boundary layer parameterization scheme for such study, which limits the simulation of typhoon. In addition, when the horizontal resolution is higher than 30km, the gradient information

15 calculated by the adjoint model has errors and omissions, which results in falling into the local optimum or optimization failure. Hence~~,~~. a ~~method~~n algorithm without using the adjoint model is needed. ~~model is needed.~~

Wen et al. (2014) proposed a modified intelligent algorithm (IAs) called SAEP (simulated annealing-based ensemble projecting method) to solve CNOP in the Zebiak-Cane (ZC) (Zebiak and Cane, 1987) model for studying the ENSO predictions. PCGD (principal components-based great deluge) (Wen et al., 2015a), RGA (robust PCA-based genetic

20 algorithm) (Wen et al., 2015b), CTS-SS (continuous Tabu search algorithm with sine maps and staged strategy) (Yuan et al., 2015), and PCAGA (principal component analysis-based genetic algorithm) (Mu et al., 2015b) also were proposed to do the same study. These ~~methods~~ algorithms were useful and effective. But it should be investigated that whether these ~~methods~~ algorithms can be used to solve CNOP in the MM5 model and WRF-ARW model for identifying sensitive areas of TTOs.

Therefore, we adopted the PCAGA to solve CNOP in the MM5 model with the 120 km horizontal resolution. The

25 experiments showed that PCAGA method was free of the adjoint model and ~~also~~ obtained CNOP~~s~~ which had similar and meaningful physical patterns with the benchmark (adjoint-based method's result~~s~~). In addition, the CNOP~~s~~ obtained by PCAGA method have more positive influence~~s~~ over the forecast improvement than by adjoint-based method (called ADJ method for short). However, the PCAGA was not paralleled and its performance ~~is~~ was ~~worse than the PPSO in the ZC model.~~not good. In our precious studies, the PPSO had better performance than the PCAGA, but it was easy to trap in local

30 optimum. Hence~~,~~. ~~we~~ combined with the advantages of particle swarm optimization (PSO) ~~and~~ and wolf search algorithm (WSA), ~~and~~ we proposed a new modified ~~IA~~algorithm, ACPW (adaptive cooperation co-evolution of parallel particle swarm optimization and wolf search algorithm based on principal component analysis) (Zhang et al., 2018). The ACPW was used to solve CNOP in the MM5 model with two horizontal resolutions, ~~60 km~~60-km and 120 km. We compared the CNOP achieved by the ACPW with ADJ-CNOP, and the experimental results showed that the ACPW-CNOP had the similar

patterns, high similarity, ~~the~~ higher benefits, less time consumption ~~faster run time~~ and the same influence on the typhoon tracks simulation. This type ~~methods~~ algorithms have not been applied to the WRF-ARW yet. WRF-ARW has more dimensions and more physical parameterizations than the MM5.

Hence, in this paper, we rewrite the ACPW ~~method~~ and applied it to solve CNOP in the WRF-ARW for identifying sensitive
5 areas of typhoons adaptive observations. We take two typhoons as study cases, Fitow (2013) and Matmo (2014), and simulate them with the ~~60 km~~60-km horizontal resolution. Similar to our previous study (Zhang et al., 2018), following the recommendation of Zhou and Zhang (2014), the total dry energy is adopted as the objective function. To evaluate the CNOPs from the ACPW method, we compare them with the benchmark in terms of the patterns, energies, similarities and benefits from the CNOPs reduced in the whole domain and sensitive regions, and the simulated typhoon tracks. All
10 experimental results show that in the WRF-ARW model the ACPW method also is feasible and effective for solving CNOPs to identify the sensitive regions of TTOs.

The rest of the paper is organized as follows. The brief description of CNOP and ACPW method is denoted in the section 2. Section 3 and section 4 are the parts of experiments, whose design is in the section 3 and analysis and results are in the section 4. The last part about the conclusions is in section 5.

15 **2 CNOP and ACPW**

2.1 CNOP

CNOP is an initial perturbation $\zeta\varphi_0^*$ of vector Φ_0 (initial basic state) under the constrain condition $\|\varphi_0\|^2 \leq \zeta$, if and only if

$$\begin{cases} J(\zeta\varphi_0^*) = \max_{\|\varphi_0\|^2 \leq \zeta} J(\varphi_{NT}) \\ \varphi_{NT} = PM(\Phi_0 + \zeta\varphi_0) - PM(\Phi_0) \end{cases}, \qquad (1)$$

20 ~~Where~~ where ζ is a constrained radius of an initial perturbation φ_0. We use $\zeta\varphi_0$ to represent the constrained initial perturbation. Φ_0 is an initial basic state and also a background field of a nonlinear numerical model. $\zeta\varphi_0$ is a type initial perturbation, which can be insert into the initial basic state Φ_0. P is a local numerical projection operator with setting 1 inside of the verification region and 0 outside, which is an operation of matrix multiplication. ~~and~~ And the verification region is a key area considered by researchers, which is represented in Fig. 1. M denotes a nonlinear numerical model.

25 Figure 1 shows the schematic diagram of verification region, which is denoted by the red square, and when model has more than one vertical level, verification region of each level is the same. In addition, different cases have different verification regions.

$$\Phi_t = M_{t_0 \to t}(\Phi_0), \qquad (2)$$

~~M denotes a nonlinear model and~~ Φ_t is the state of nonlinear evolution~~propagator~~ of M from the initial time t_0 to the
30 predicted time t. Combined with the formula (2), the formula (1) means that the CNOP is the initial perturbation having

largest nonlinear development, i.e. $J(\zeta\varphi_0^*)$, when it is inserted into Φ_0 and M evolves from the initial time t_0 to the predicted time t with the modified initial state $(\Phi_0 + \zeta\varphi_0)$. J denotes the objective function of solving CNOP, and the detail of its computation is described in Section 3. Because, the detail of calculating J would be different as the experimental design is different.

We convert the objective function $J(\zeta\varphi_0^*)$ to a problem of seeking minimum.

$$J(\zeta\varphi_0^*) = \min_{\|\varphi_0\|^2 \leq \zeta} -J(\varphi_{NT}), \tag{3}$$

2.2 ACPW

The ACPW method was proposed by Zhang et al. (2018), which is used to solve CNOP in the MM5 model for identifying the sensitive regions of TTOs. The ACPW has two points, one is the cooperation co-evolution of PSO and WSA, the other is the two adaptive subswarms. The details and pseudocode of ACPW is described in Table 1. And the control parameters of ACPW are list in Table 2.

The update rules ~~elaborations~~ of the PSO and WSA ~~update rules were in the study of Zhang et al. in 2018 (Zhang et al., 2018)~~are descripted in the following.

The PSO use the classical formula (4) to update the individuals.

$$\begin{cases} v_i^{k+1} = \omega v_i^k + c_1\alpha(o_i^k - u_i^k) + c_2\beta(o_g^k - u_i^k) \\ u_i^{k+1} = u_i^k + \gamma v_i^{k+1} \end{cases} \tag{54}$$

where~~,~~ ~~the~~ superscript k is the current iteration and ~~k or~~ $k + 1$ is the next iterative step~~.~~ v_i^{k+1} is the updating velocity of the individual u_i^k ~~and calculated by the first subformula~~. ω ~~is~~ is the inertia coefficient~~.~~ c_1 is the learning factor for self-awareness to track the historically optimal position, and c_2 ~~are the learning factors~~for social-awareness of the particle swarm to track the globally~~.~~ α and β are the random numbers uniformly distributing ~~on~~in (0, 1) ~~the interval from 0 to 1~~. o_i^k is the local optimum and o_g^k is the global optimum in the kth iteration. γ is the restraint factor to control the speed. u_i^{k+1} is the updated individual ~~with PSO~~.

There are two ways for updating individual in WSA, prey and escape, which represent the functions of searching in a local region and escaping from a local optimum.

$$\begin{cases} u_i^{k+1} = u_i^k + \theta \cdot r \cdot rand(\ ) & dist(u_i^k, u_i^{k+1}) < r.\,and.\,J(u_i^k) < J(u_i^{k+1}) \\ u_i^{k+1} = u_i^k + \theta \cdot s \cdot escape(\ ) & p > p_a \end{cases} \tag{65}$$

where the superscript k or k + 1 is also the iterative step, θ is the velocity, r is the local optimizing radius, which smaller than the global constraint radius δ. $rand()$ is the random function, whose mean value distributed in [-1,1]. $escape ()$ is the

4

function of calculating a random position, which is larger 3 times than r. s is the step size of the updating individual. p is a random number in $[0,1]$, p_a is the probability of individual escaping from the current position.

The elaborations of the PSO and WSA update rules were in the study of Zhang et al. in 2018 (Zhang et al., 2018).

3 Experimental Design

All the experiments are run on a Lenove Thinkserver RD430 with two Intel Xeon E5-2450 2.10 GHz CPUs, 32 logical cores and 132G RAM. And the operating system is CentOS 6.5. All the codes are written in FORTRAN language and compiled by PGI Compiler 10.2.

3.1 The model and Data

In this paper, we adopt the WRF-ARW model and its corresponding adjoint system (Zhang et al., 2013) to study the sensitive areas identification of TTOs. We produce the initial and boundary conditions by using the FNL (Final Analysis) data from NCEP (National Centers for Environmental Prediction) (NCEP, 2000) at 1 °×1 °and 6-h intervals. The physical parameterization schemes of the WRF-ARW are constructed as dry convective adjustment, the surface drag planetary boundary layer scheme, grid resolved large-scale precipitation and the Kuo cumulus parameterization scheme. We also use observed typhoon tracks (Ying et al., 2014) from the China Meteorological Administration (CMA) - Shanghai Typhoon Research Institute to evaluate the simulated typhoon tracks of the WRF-ARW model.

3.2 Typhoons Fitow (2013) and Matmo (2014)

We take two typhoons as the study cases, Fitow (2013) and Matom (2014). Fitow is the 23st typhoon of 2013, and develop on September 29 to the east of Philippines. On October 6, Fitow strikes China at Fuding in Fujian province, with a landfall pressure of 955 hPa. Typhoon Matmo (2014) is the 10th typhoon of 2014. It initially happened on July 17 and made landfall in Taiwan on July 22. In these two cases, a set of 24-h control forecasts, which served as basic state, are investigated from 0000 UTC 5 Oct 2013 to 0000 UTC 6 Oct 2013 (Fitow), and from 1800 UTC 21 Jul 2014 to 1800 UTC 22 Jul 2014 (Matom). During these 24 hours, the maximum sustained winds up to 45 meters per second for typhoon Fitow and 42 meters per second for Matmo, before the typhoons hits land. For each case, the forecast is executed at a 60-km resolution with 21 vertical levels with the top pressure at 50hPa, and the model domain covers 55×55 grids.

The simulated typhoon tracks of WRF-ARW model are presented in Fig. 2. The ability of the WRF-ARW model simulating these cases accurately are checked built on a 24-h simulation initialized at 0000 UTC 5 Oct 2013 and 1800 UTC 21 Jul 2014. Figure 2(a) shows the model simulated track of typhoon Fitow (hollow) runs a little faster than the observed track (solid) and moves to the south after 0012 UTC 05 Oct 2013. Figure 2(b) shows the model simulated track of typhoon Matmo (hollow)

带格式的：字体：（中文）+中文正文（宋体），（中文）中文(中国)

moves along the observed track (solid) but slightly faster, and after 6 hours has a little migration. All these errors are acceptable in this study.

3.3 Experimental setup

As the conducted physical parameterization schemes, we only focus on the dry physical process in this paper. Therefore, the initial perturbation $\zeta\varphi_0$ related to four dry physical characteristics, i.e., the perturbed zonal wind u'_0, meridional wind v'_0, temperature T'_0 and surface pressure p'_{s0}. The objective function is calculated by the total dry energy (Zhou and Zhang, 2014) in formula (46).

$$J(\varphi_{NT}) = \frac{1}{D}\int_D \int_0^1 \frac{1}{2}\left(u_t'^2 + v_t'^2 + \frac{c_p}{T_r}T_t'^2\right)d\eta dD + \frac{1}{D}\int_D R_a T_r \left(\frac{p'_{st}}{p_r}\right)^2 dD, \qquad (46)$$

where u'_t, v'_t, T'_t, p'_{st} are components of φ_{NT}, which is the nonlinear development of perturbed Φ_0 (i.e. $\Phi_0 + \zeta\varphi_0$) from the initial time t_0 to the prediction time t. η is the vertical coordinate. D is the verification area. And other reference parameters with constant values are shown in Table 3.

For optimizing conveniently, the ~~formula~~ objective function of solving CNOP in formula (3) can be expressed~~transformed~~ to ~~solve a minimization problem, as follows~~formula (7):

$$J(\zeta\varphi_0^*) = \min_{\|\varphi_0\|^2 \le \zeta}\left(-\frac{1}{D}\int_D \int_0^1 \frac{1}{2}\left(u_t'^2 + v_t'^2 + \frac{c_p}{T_r}T_t'^2\right)d\eta dD + \frac{1}{D}\int_D R_a T_r \left(\frac{p'_{st}}{p_r}\right)^2 dD\right), \qquad (57)$$

4. Experimental Results and Analysis

To verify the feasibility and validity of the ACPW in the WRF-ARW model, we compare CNOPs obtained with those from the ~~ADJ method~~ADJ method in terms of the pattern, energy, similarity, benefits from the CNOPs reduced in the whole domain and sensitive regions, as well as the simulated typhoon tracks.

4.1 CNOP pattern

The pattern is the most important standard among the evaluation standards for CNOP, especially the pattern of the vertical dry energy, because the sensitive areas are identified by the large energy.

The CNOP patterns of ADJ-CNOP and ACPW-CNOP of the WRF-ARW are denoted in the Figures 3 and 4. Figure 3 is for typhoon Fitow, and typhoon Matmo is shown in Figure 4. The shaded parts represent the temperature and the vectors describe the wind. The patterns are the vertical level at $\eta = 0.7$, i.e. the 500 hPa atmospheric layer, which is focused on by researchers generally. From the figures, we can find that the patterns of ACPW-CNOP is similar to those of the ADJ-CNOP in all typhoons. The distribution of warm and cold temperature zones is approximately the same, and the direction of wind

vector is almost the same. Except for the CNOP patterns of ACPW are more dispersed and fragmented than those of ~~ADJ-method~~ADJ method.

As we use the total vertical dry energy to identify the sensitive regions of typhoons, the distribution of the vertical dry energy is presented in Figure 5 and Figure 6. And the figures show the area with the first 1.2% energy.

5   For typhoon Fitow, the energy almost has the same position, which is distributed in the north side of the verification area. The difference is the ACPW-CNOP has another secondary part in the southeast side of the verification area.

However, the energy position of ACPW-CNOP is different with the ADJ-CNOP for typhoon Matmo in Figure 6. The energy distribution of these two ~~CNOPs~~ CNOPs are concentrated in two blocks, but the deviation of the position is large. The energy of ADJ-CNOP is mainly distributed in the southwest and east side of the verification area. One major part in the east

10 side is crescent-shaped with large power, and the other one in the southwest has smaller energy than the former. The energy of ACPW-CNOP distributes in the northwest and northeast of the verification area, which has the similar power.

To sum it up, the distribution of CNOP pattern is more similar then that of the CNOP energy, and under the condition of the 60-km resolution, the similarity of upon distribution is higher than those in the MM5 model of the paper published by Zhang et al. in 2018 (Zhang et al., 2018).

15

In order to further analyze the similarity and the forecasting benefit of the identified sensitive region, the following numerical analysis experiments are carried out in this paper.

4.2 Numerical similarity

The numerical similarity between ACPW-CNOP and ADJ-CNOP is calculated by formula (~~6~~8).

20
$$S_{xy} = \frac{\langle X,Y \rangle}{\sqrt{\langle X,X \rangle}\sqrt{\langle Y,Y \rangle}},$$
(~~6~~8)

X and Y represent the vectors of CNOPs obtained from the ACPW and ~~ADJ method~~ADJ method. The similarity values are list in Table 4.

0.61 is the similarity value of the two CNOPs of Typhoon Fitow, and 0.53 is for typhoon Matmo. Compare to the pattern similarity in Figures 3 and 4, the numerical similarity is smaller. It is because that the pattern is plotted by the values of one

25 vertical level, while the numerical similarity is calculated by the all values of CNOP including all physical quantities and vertical levels. Even so, the similarity values also are more than 0.5.

4.3 Benefits from reduction of CNOPs

The experiments of this section include two parts: the forecasting benefits obtained by reducing CNOP to W × CNOP in the whole domain, i.e. the CNOP values of all grid points are reduced; the forecasting benefits from CNOP to W × CNOP is

30 reduced only in the sensitive regions, i.e. the CNOP values of the sensitive grid points are reduced to 0.75 × CNOP, 0.5 × CNOP ~~and~~ and 0.25 × CNOP.

All experiments are based on two assumptions that:

a. When adding target observations in the identified sensitive areas, the environment around is idealized, and the improvements of observations added are reducing original errors to 0.75, 0.5 and 0.25 times.

b. CNOPs achieved by us can be seen as the optimal initial perturbations. Once we reduce them in the sensitive regions, the benefits earned will be the best.

As mentioned in the subsection 4.1, the sensitive region is determined according to the first 1.2% of total vertical dry energy, as shown in Figures 5 and 6, which are the shadow zones in the figures.

4.3.1 Reducing CNOP to W × CNOPs in the whole domain

Figure 7 shows the forecasting benefits of reducing CNOP to W × CNOPs in the whole domain of ADJ-CNOP and ADJ-CNOP.

From Figure 7, we can see that the forecasting benefits of ACPW-CNOP is greater than that of ADJ-CNOP in typhoon Fitow, while the result is opposite in typhoon Matmo.

4.3.2 Reducing CNOP to W × CNOPs in the sensitive regions

The sensitive regions of TTOs are identified by ~~the~~ upon strategy for selecting points, which are plotted in the Figures 5 and 6. The forecasting benefits are list in Table 5.

From the numerical results in Table 5, it can be seen that the forecast ~~income~~benefit of ACPW-CNOP in the sensitive region is greater than that of ADJ-CNOP in all typhoons. Especially, the benefits of ACPW-CNOP are much larger than those of ADJ-CNOP, ~~and~~ which is two orders of magnitude larger than the latter.~~the gap is two orders of magnitude.~~ In addition, when the W coefficient of ADJ-CNOP decreases gradually, the forecast ~~income~~benefit of ADJ-CNOP keeps basically unchanged, about 6.9% in typhoon Fitow and about 0.08% in typhoon Matmo. While the forecast benefit of ACPW-CNOP changes obviously. The benefit ~~value~~ of typhoon Fitow is 10.2871%, 9.6823%, 8.8120% respectively, and typhoon Matmo is 2.3484%, 3.5716% and 5.2212% respectively.

4.4 Efficiency analysis

As the efficiency analysis of solving CNOP in the MM5 model (Zhang et al., 2018), the time consumption of solving CNOP by ACPW belongs to the times of calling the non-linear model. From the experiments, the time consumption of the non-linear model of WRF-ARW is more than that of the MM5. Hence, we must consider the influence from the values of the control parameters of the ACPW, such as the number of principle ~~components~~ components n', the number of individuals N and the number of iterations $Total\_Step$.

In this subsection, we set several group values of upon three control parameters to investigate the time consumption of ACPW, ~~and.~~ ~~the~~ The other parameters are the same ~~to~~ as those in Table 2. The time consumption ~~The running time~~ is list in

Table 6 under the condition ~~of~~ that the WRF-ARW model is run paralleled ~~ning WRF-ARW~~ with 32 logical cores ~~parallelly~~. In addition, the time consumption value ~~the running time~~ is the average ~~value~~ of four experiments ~~under the same conditions~~. The average time consumption~~running time~~ of ADJ method is 232.31 minutes~~,~~. As the SPG2 needs to execute several times to find the best result, several different initial perturbations (also called first guess fields) are needed. In this paper, we use four first guess fields. And when we use the four first guess fields, ~~and~~ the time consumption ~~total running time~~ of ADJ method ~~using four initial first guess fields~~ is up to 929.24 minutes. All the results are based on the Fitow case. The Matmo case has similar results.

Eight ~~representative~~ group of control parameters and the experimental results are list in Table 6. F~~r~~om the experimental analysis, the number of principal components (PCs), ~~i.e.~~ which are selected dimensions of the feature space from the dimension reduction of Principal Component Analysis (PCA), has little effect on the time consumption ~~running time~~, but has great influence on the adaptive value of objective function. The samples of PCA are from the difference of the different forecast states at the forecast time. In the WRF-ARW model, we get 551 samples and reduce the dimension from $2.5*10^5$ to 30-60 with PCA.~~.~~

When the number of individuals and iteration steps remain unchanged but the dimension setting increases gradually, the adaptive value of objective function of ACPW-CNOP decreases gradually, referring to lines 5 and 7 of Table 6. This is due to the increasing dimension needs more individual and iterations to optimize in the feature space, if not it will resulte in the method falling into a local optimum.

It also can be seen that the ~~running time~~time consumption of ACPW is proportional to the number of $N \times Total\_Step$. When the number of $N \times Total\_Step$ is the same, the ~~running time~~time consumption of ACPW is almost the same. When the number of $N \times Total\_Step$ is increased, the ~~running~~ time consumption also increases proportionally. Moreover~~, , from line 1 to line 3 of the values,~~ it is found that the increasing individuals does not make the objective function value larger in lines 1-3~~increase the adaptive values~~. In lines 2-4,~~From line 2 and line 4 of the values,~~ the number of iterations is increased, the adaptive values ~~increase~~get larger. In here, to understand conveniently, we list the positive objective function values in Table 6 while the outputs of the program are negative. We ~~We~~ can conclude that the increasing iterations is beneficial to the optimization of the ACPW.

~~Observing the adaptive values~~For Table 6, it is found that the objective function values ~~of~~in lines 4 and ~~line~~ 6 are more than 30000, and the corresponding ~~running time~~time consumption is about 360 minutes. When we use the parameters of line 1, the ~~adaptive~~ objective function value is 28126.185933, which is little smaller than 30000, but its time consumption~~running time~~ is only 89.83 minutes~~, and the benefits are in Figures 7~~. And the identified sensitive areas are not much different. Therefore, we use the parameters in line 1 to do the experiments. ~~we can set some small number of the control parameters to do the experiments.~~ When using the parameters in line 1 and the ~~ADJ method~~ADJ method using one first guess field, the speedup of the ACPW is 2.59. The time consumption of ADJ method divided by the time consumption of ACPW is the speedup of the ACPW.~~.~~ ~~If~~If the ADJ~~ method uses four first guess fields, the speedup of the ACPW is 10.34. In this paper, the ACPW is more efficient than the ~~ADJ method~~ADJ method.

4.5 Simulation of the typhoon tracks

In order to investigate the validity of CNOP in identifying sensitive regions, we compare the 24-hour simulated typhoon track by adding CNOP or W × CNOP to the initial states. Similar to the benefits, there are two ways to modify the CNOP value: one is to reduce the CNOP value to 0.75, 0.5 and 0.25 times in the whole domain; the other is to reduce the CNOP value to 0.5 times only in the sensitive regions of TTOs.

In order to show the effect clearly, only two tracks are drawn in each sub-figure, one is the best typhoon track provided by CMA, and the other is the simulation track of the WRF-ARW model with different CNOPs, as shown in Figures 8 and 9. Since the difference of typhoon tracks simulated by the WRF-ARW model after adding modified CNOPs is very small, it is difficult to find them when they are displayed in the figures. Therefore, the experimental results of this part are also shown in Tables 7 and 8 ~~in a numerical way~~. The larger values in the tables are longitude (E) and the smaller values are latitude (N).

4.5.1 Simulated track analysis of adding CNOP modified in the whole domain

Firstly, we ~~analyse~~analyze the simulated Fitow tracks of the WRF-ARW model after adding modified ADJ-CNOP ~~in the whole domain~~ to the initial state in the whole domain, and the results are ~~shown~~showed in Figures 8 and 9.

Combining with the tracks in Figure 8 and the data in Table 7, it can be seen that the track~~s~~ of typhoon Fitow ~~has~~have ~~two~~little difference~~s, which is simulated by the WRF-ARW model after reducing the value of CNOP in the whole domain and adding it on the initial state. One difference.~~ One is the position of simulated typhoon tracks at 1200 UTC 5 Oct.~~. Only and~~ the position with adding the whole ADJ-CNOP is different with that of adding another W×ADJ-CNOPs.~~.~~ The other ~~The second~~ difference is the position of 0.5×CNOP and 0.25×CNOP at 1800 UTC 5 Oct. The other positions are the same. In addition, it is obvious that the Fitow track has great error after adding modified CNOPs to the initial state, which indicates that the quality of the initial state is deteriorated by CNOP ~~superimposition~~, and the forecasting error is increased.

Different to typhoon Fitow, all simulated tracks of typhoon Mamto are different, which are shown in Figure 9. The track data is list in Table 8.

In the Figure 9, we can see that when the modified ADJ-CNOP is inserted into the initial state, the typhoon Matmo tracks simulated ~~from~~by the WRF-ARW model are closer to the observed track ~~by inserting the modified ADJ-CNOP to the initial state, which is only simulated by the WRF-ARW of Figure 2 (b)~~. The reason is that there is a big difference between the WRF-ARW simulated track and the observed track. ~~That is to say,~~ It means that the quality of the initial state is not very well, ~~which~~and that results in a forecast error. The action of adding errors improves the initial state instead, which makes the forecasting track error smaller. This result also provides a new idea for the application of CNOP method in the typhoon track simulation research.

Except the position at 1800 and 0000 UTC 21 Jul, the track data is all different, especially at 1800 UTC 22 Jul. ~~Analysis combining with~~For the Figure 9, when all CNOP is retained, the position at 1800 UTC 22 Jul is the furthest from the observed position, and as the decreased CNOP, it moves to the observed position. The results also prove the sensibility of CNOP.

5 ~~Next, t~~The influence of the ACPW-CNOP on the simulated typhoon track also is ~~analysed~~analyzed. The tracks are drawn in Figures 10 and 11, and position data also is list in Tables 6 and 7. For typhoon Fitow, four sub-figures of the Figure 10 are the same, because the different ACPW-CNOPs have the same influence on the simulated typhoon tracks.

For typhoon Matmo, there are two same sub-figures, i.e. Figure 11 (b) and (c), and two different sub-figures, i.e. Figure 11 (a) and (d). And the different position is the initial position at 1800 UTC 21 Jul and the end position at 1800 UTC 22 Jul.

10 Moreover, the difference of data is little.

Comparing the effects of ADJ-CNOP and ACPW-CNOP on typhoon track simulation, it is found that for Fitow case, the two CNOPs have the similar effect on typhoon track~~,.~~ ~~while~~ While for Matmo case, the influence of ACPW-CNOP is less than that of ADJ-CNOP. The typhoon track generated by adding ACPW-CNOP is very close to that simulated track of the WRF-ARW model (Figure 2 (b)), but much closer to the observed typhoon track.

15 **4.5.2 Simulated track analysis of adding CNOP modified in the sensitive regions of TTOs**

After reducing CNOPs in the sensitive regions ~~of TTOs~~ identified by ~~ADJ-method~~ADJ method and ACPW, the typhoon tracks are ~~shown~~ showed in Figures 12 and 13, which are simulated by the WRF-ARW model with adding modified CNOPs to the initial state. The strategy of reducing CNOP is change the values to 0.5 time only in the sensitive regions. The ~~tracks~~ position data can be seen in Tables 7 and 8.

20 ~~The analysis results of Figure 10 and Figure 11 are consistent with those above, that is, i~~In Fitow case, the sensitive regions identified by ACPW-CNOP and ADJ-CNOP have the similar influence on typhoon track simulation; in Matmo case, the sensitive regions identified by ACPW-CNOP have less influence than ADJ-CNOP, but when adding the observations in the sensitive regions, i.e. reducing the CNOP values in the sensitive regions, the simulated tracks are better than those simulated by the WRF-ARW model (Figure 2 (b)).

25 In conclusion, the sensitive regions identified by the ACPW-CNOP has the similar influence with the ADJ-CNOP on the simulation of typhoon tracks, sometimes the ACPW-CNOP has more positive impact on the simulation of typhoon tracks.

5 Summaries and Conclusions

In this paper, we rewrite the ACPW and applied it to solve CNOP in the WRF-ARW for identifying sensitive areas of TTOs, which is proposed by us in the study of Zhang et al. (2018), to investigate its feasibility and effectiveness in the WRF-ARW

30 model. We take two typhoons as study cases, Fitow (2013) and Matmo (2014), and simulate them with the ~~60 km~~60-km horizontal resolution. ~~Similar to our previous study (Zhang et al., 2018), t~~The total dry energy is adopted as the objective

function. The CNOP is also calculated by the ~~ADJ method~~ADJ method as the benchmark. To evaluate the ACPW-CNOP, five aspects are analysed, such as the pattern, energy, similarity, benefits from the CNOPs reduced in the whole domain and the sensitive regions identified, and the simulated typhoon tracks.

Based on the experimental results, the following conclusions can be drawn:

(1) The temperature and wind patterns of ACPW-CNOP is similar to those of the ADJ-CNOP in all typhoons. The distribution of temperature zones and the direction of wind vector is almost the same. Except for the CNOP patterns of ACPW are more dispersed and fragmented than those of ~~ADJ method~~ADJ method.

(2) The similarity values of ADJ-CNOP and ACPW-CNOP of two typhoon cases are more than 0.5. The Fitow is 0.61, and the Matmo is 0.53.

(3) When reducing CNOPs in the whole domain, the forecasting benefits of ACPW-CNOP is greater than that of ADJ-CNOP in typhoon Fitow, while the result is opposite in typhoon Matmo. When reducing CNOPs in the sensitive regions, the forecast ~~income~~benefit of ACPW-CNOP is greater than that of ADJ-CNOP in all typhoons.

(4) When ACPW uses the parameters in line 1 of Table 6 and the ~~ADJ method~~ADJ method uses one first guess field, the speedup of the ACPW is 2.59. If the ~~ADJ method~~ADJ method uses four first guess fields, the speedup of the ACPW is 10.34. ~~In the experiments of this paper, t~~The ACPW is more efficient than the ~~ADJ method~~ADJ method in this paper.

(5) The sensitive regions identified by the ACPW-CNOP has the similar influence with the ADJ-CNOP on the simulation of typhoon tracks, sometimes the ACPW-CNOP has more positive impact on the simulation of typhoon tracks.

Overall, the feasibility and effectiveness of ACPW is proved in the WRF-ARW model.

To ~~compared~~compare with the ~~ADJ method~~ADJ method, it is limited when we construct the physical parameterization schemes of WRF-ARW. Because the corresponding adjoint model only provides one physical parameterization scheme. And that may be the reason of bad simulated Fitow typhoon track. Since the ACPW method is free of the adjoint model, we will try more complicated physical parameterization schemes and improve the horizontal resolution to do such research. Moreover, ACPW can be used to solve CNOP in the numerical models no having adjoint model, such as GFDL (Geophysical Fluid Dynamics Laboratory) and CESM (Community Earth System Model).

References

Aberson, S. D.: Targeted Observations to Improve Operational Tropical Cyclone Track Forecast Guidance, Mon. Wea. Rev., 131(131), 1613, 2003.

Bergot T.: Adaptive observations during FASTEX: A systematic survey of upstream flights, Quart. J. Roy. Meteor. Soc., 125(561), 3271-3298, 1999.

5 Dee, D. P., and 35 co-authors.: The ERA-Interim reanalysis: Configuration and performance of the data assimilation system, Quart. J. Roy. Meteor. Soc., 137, 553-597, 2011.

Ernesto G. Birgin, Marcos Raydan. Algorithm 813: SPG - Software for Convex - Constrained Optimization. ACM Transactions on Mathematical Software (TOMS), 27(3), 340-349, 2001.

Franklin, J. L., and Demaria, M.: The Impact of Omega Dropwindsonde Observations on Barotropic Hurricane Track
10 Forecasts, Mon. Wea. Rev., 120(120), 381-391, 1992.

Mu, B., Wen, S., Yuan, S., and Li, H.: PPSO: PCA based particle swarm optimization for solving conditional nonlinear optimal perturbation, Comput. Geosci., 83, 65-71, 2015a.

Mu, B., Zhang, L., Yuan, S., and Li, H.: PCAGA: principal component analysis based genetic algorithm for solving conditional nonlinear optimal perturbation, in: 2015 International Joint Conference on Neural Networks (IJCNN), IEEE,
15 Ireland, 12-17 July 2015, 1-8, 2015b.

Mu, M., and Duan, W. S.: A new approach to studying ENSO predictability: Conditional nonlinear optimal perturbation, Chinese Sci. Bul., 48, 1045-1047, 2003.

National Centers for Environmental Prediction/National Weather Service/NOAA/U.S. Department of Commerce (2000), NCEP   FNL   Operational   Model   Global   Tropospheric   Analyses,   continuing   from   July   1999,
20 https://doi.org/10.5065/D6M043C6, Research Data Archive at the National Center for Atmospheric Research, Computational and Information Systems Laboratory, Boulder, Colo. (Updated daily.)

Skamarock, W. C., and Coauthors,: A description of the Advanced Research WRF version 3. NCAR Tech. Note NCAR/TN-4751STR. 113 pp., 2008.

Wen, S., Yuan, S., Mu, B., Li, H., and Ren, J.: PCGD: Principal components-based great deluge method for solving CNOP,
25 in: Evolutionary Computation (CEC), 2015 IEEE Congress on. IEEE, 25-28 May 2015, 1513-1520, 2015a.

Wen, S., Yuan, S., Mu, B., Li, H., and Chen L.: SAEP: Simulated Annealing Based Ensemble Projecting Method for Solving Conditional Nonlinear Optimal Perturbation, in: Algorithms and Architectures for Parallel Processing, 14th international conference, ICA3PP 2014, Dalian, China, 24–27 August 2014, 655-668, 2014.

Wen, S., Yuan, S., Mu B, and Li, H.: Robust PCA-Based Genetic Algorithm for Solving CNOP, in: Intelligent Computing
30 Theories and Methodologies, 11th International Conference, ICIC 2015, Fuzhou, China, 20-23 August 2015, 597-606, 2015b.

Ying, M., Zhang, W., Yu, H., Lu, X., Feng, J., Fan, Y., Zhu, Y., and Chen, D.: An overview of the China Meteorological Administration tropical cyclone database, J. Atmos. Oceanic Technol. (31), 287-301, 2014.

Yuan, S., Qian, Y., and Mu, B.: Paralleled Continuous Tabu Search Algorithm with Sine Maps and Staged Strategy for Solving CNOP, in: Algorithms and Architectures for Parallel Processing, 15th International Conference, ICA3PP 2015, Zhangjiajie, China, 18-20 November 2015, 281-294, 2015.

Yu H, Wang H, Meng Z, et al. A WRF-Based Tool for Forecast Sensitivity to the Initial Perturbation: The Conditional Nonlinear Optimal Perturbations versus the First Singular Vector Method and Comparison to MM5. Journal of Atmospheric & Oceanic Technology, 34(1), 186-206, 2017.

Zebiak, S.E., Cane, M.A.: A Model El Niño-Southern Oscillation. Mon. Wea. Rev., 10(115), 2262-2278, 1987.

Zhang, L. L., Yuan, S. J., Mu, B., and Zhou F. F.: CNOP-based sensitive areas identification for tropical cyclone adaptive observations with PCAGA method, Asia-Pac. J. Atmos. Sci., 53(1), 63-73, 2017.

Zhang L, Mu B, Yuan S, et al. A novel approach for solving CNOPs and its application in identifying sensitive regions of tropical cyclone adaptive observations. Nonlinear Processes in Geophysics, 25(3), 693-712, 2018.

Zhang X, Huang X Y, and Pan N. Development of the upgraded tangent linear and adjoint of the Weather Research and Forecasting (WRF) model. J. Atmos. Oceanic Technol., 30, 1180–1188, 2013.

Zhou, F., and Mu, M.: The impact of verification area design on tropical cyclone targeted observations based on the CNOP method, Adv. Atmos. Sci., 28(5), 997-1010, 2011.

Zhou, F., and Mu, M. The Impact of Horizontal Resolution on the CNOP and on Its Identified Sensitive Areas for Tropical Cyclone Predictability, Adv. Atmos. Sci., 29(01), 36-46, 2012a.

Zhou, F., and Mu, M.: The Time and Regime Dependencies of Sensitive Areas for Tropical Cyclone Prediction Using the CNOP Method, Adv. Atmos. Sci., 29(04), 705-716, 2012b.

Zhou, F., and Zhang, H.: Study of the Schemes Based on CNOP Method to Identify Sensitive Areas for Typhoon Targeted Observations, Chinese J. Atmos. Sci. (2), 261-272, 2014.
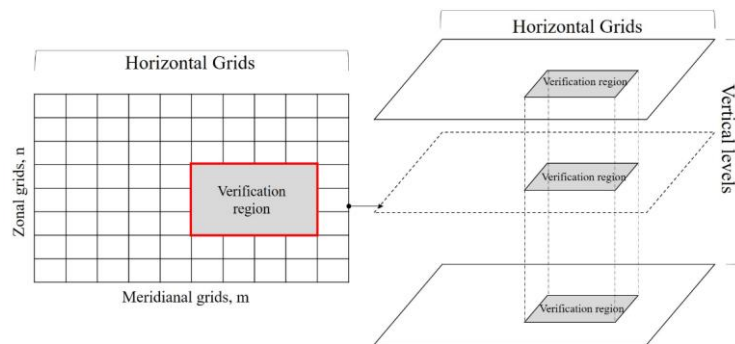
Figure 1: The schematic diagram of verification region. The red square represents the verification region, m is the number of meridional grids and n is the number of zonal grids in horizontal grids.
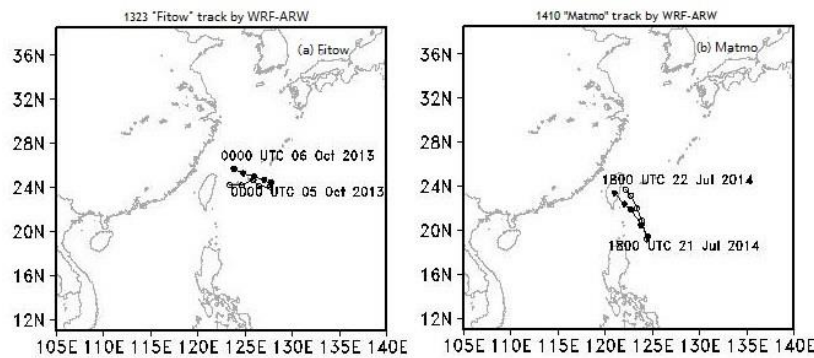

Figure 2: Simulated tracks of WRF-ARW model and typhoon observed tracks of CMA. Solid circles represent typhoon observed tracks of CMA, hollow circles show simulated tracks. (a) Fitow from 0000 UTC 5 Oct to 0000 UTC 6 Oct 2013. (b) Matmo from 1800 UTC 21 Jul to 1800 UTC 22 Jul 214.
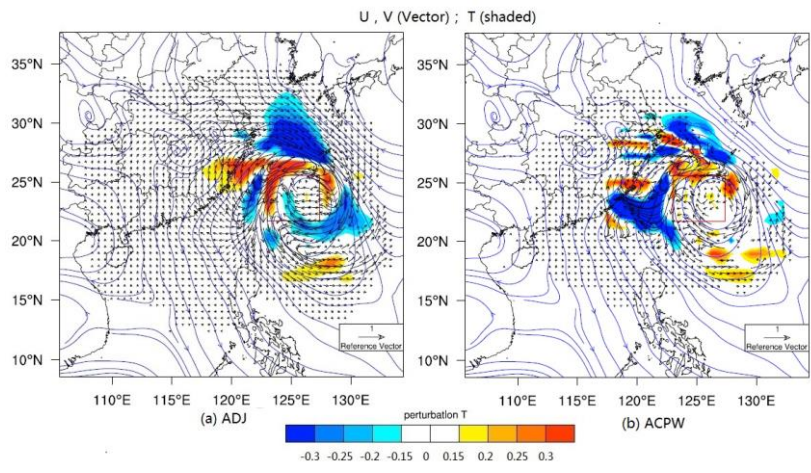
15

Figure 3: The CNOP patterns of Fitow at $\eta = 0.7$. The shaded parts represent the temperature (units: K) and the vectors describe the wind (units: ms-1). The squares draw the verification areas. (a) denotes the CNOP pattern of the ~~ADJ-method~~ADJ method and (b) presents the ACPW.
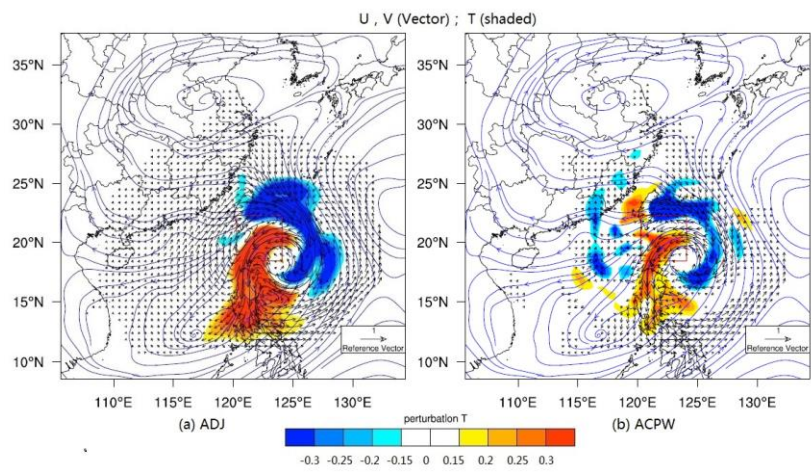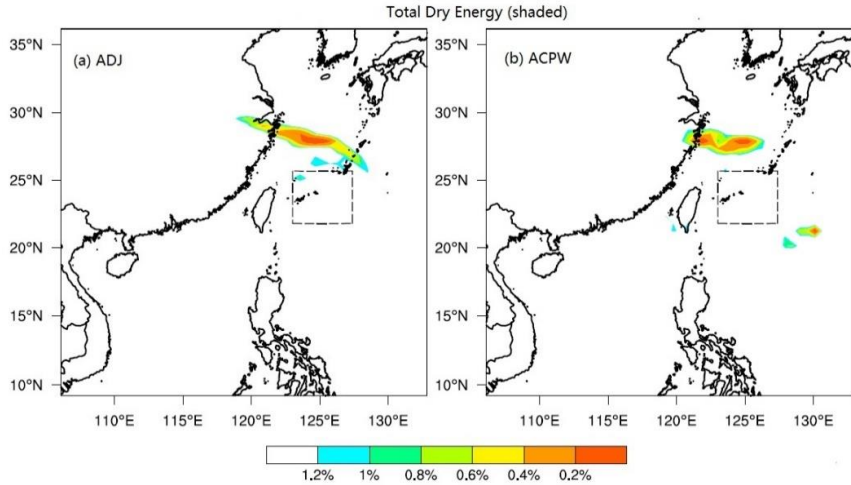

5

Figure 4: The CNOP patterns of Matmo at $\eta = 0.7$. The shaded parts represent the temperature (units: K) and the vectors describe the wind (units: ms-1). The squares draw the verification areas. (a) denotes the CNOP pattern of the ~~ADJ method~~ADJ method and (b) presents the ACPW.

5   **Figure 5: Same as Figure 3, but the shaded parts represent the vertically integrated energies for Fitow (units: J kg-1), and the black virtual box represents the validation area.**
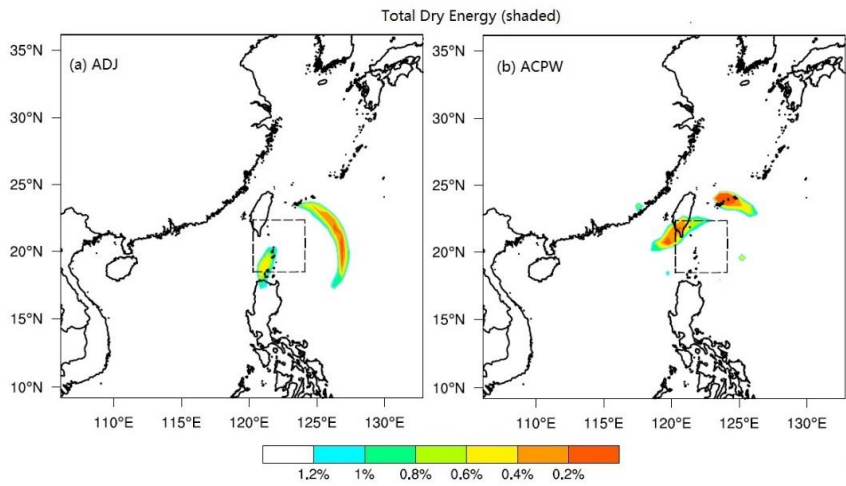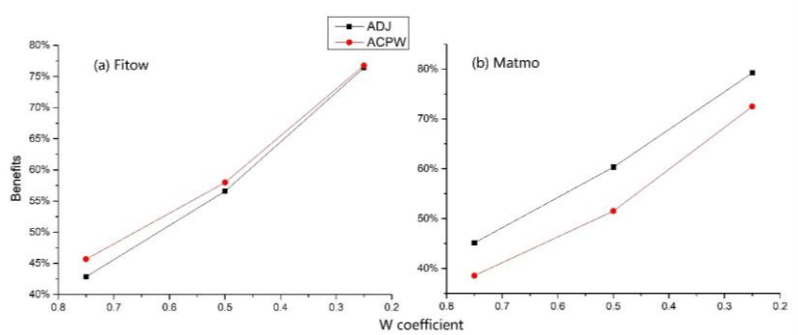
Figure 6: Same as Figure 4, but the shaded parts represent the vertically integrated energies for Fitow (units: J kg-1), and the black virtual box represents the validation area.

5   Figure 7: Benefits (percent, %) achieved by reducing CNOPs to W×CNOPs of ADJ and ACPW methods in the whole domain for typhoon Fitow (2013). The x-coordinate is the W coefficient values. And the y-coordinate denotes the benefits (percent, %) derived from the two methods. ~~ADJ method~~ADJ method is described as black line with squares and ACPW is red line with circles.

Figure 8: Simulated typhoon tracks of WRF-ARW with adding ADJ-CNOP or W×ADJ-CNOP into the initial state in the whole domain for Fitow. Solid circles represent observed tracks of CMA, and hollow circles show the simulated tracks of the WRF-ARW model. (a), (b), (c) and (d) denote CNOP, 0.75×CNOP, 0.5×CNOP and 0.25×CNOP, respectively.
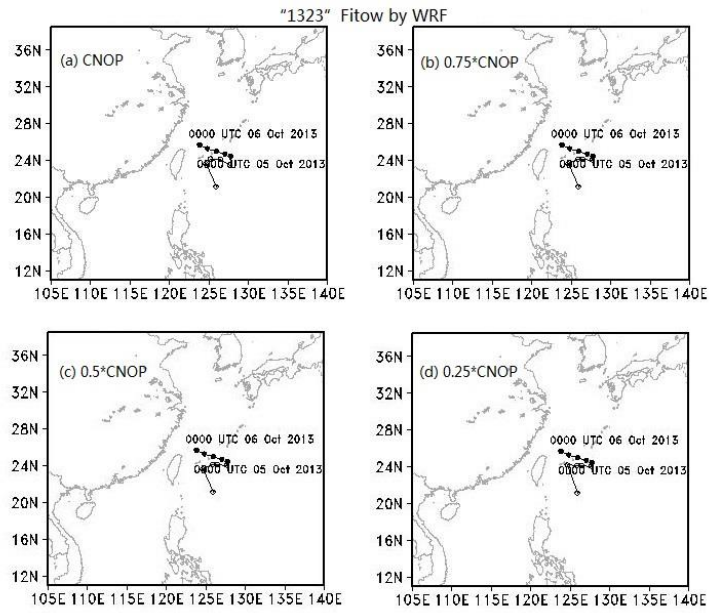
Figure 9: Simulated typhoon tracks of WRF-ARW with adding ADJ-CNOP or W×ADJ-CNOP into the initial state in the whole domain for Matmo. Solid circles represent observed tracks of CMA, and hollow circles show the simulated tracks of the WRF-ARW model. (a), (b), (c) and (d) denote CNOP, 0.75×CNOP, 0.5×CNOP and 0.25×CNOP, respectively.
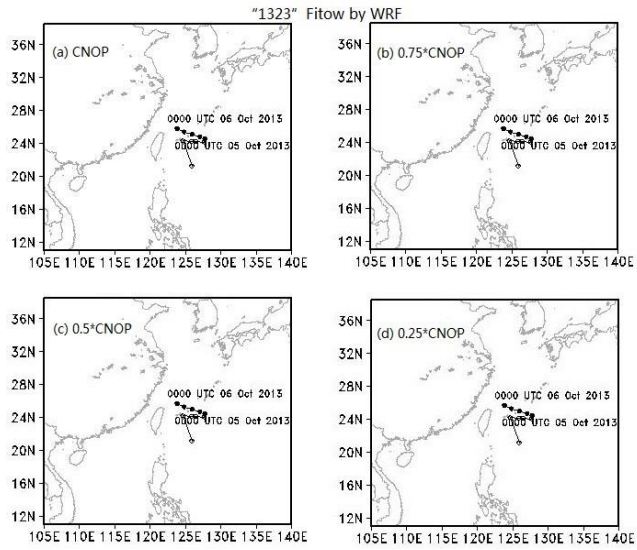
Figure 10: Simulated typhoon tracks of WRF-ARW with adding ACPW-CNOP or W×ACPW-CNOP into the initial state in the whole domain for Fitow. Solid circles represent observed tracks of CMA, and hollow circles show the simulated tracks of the WRF-ARW model. (a), (b), (c) and (d) denote CNOP, 0.75×CNOP, 0.5×CNOP and 0.25×CNOP, respectively.
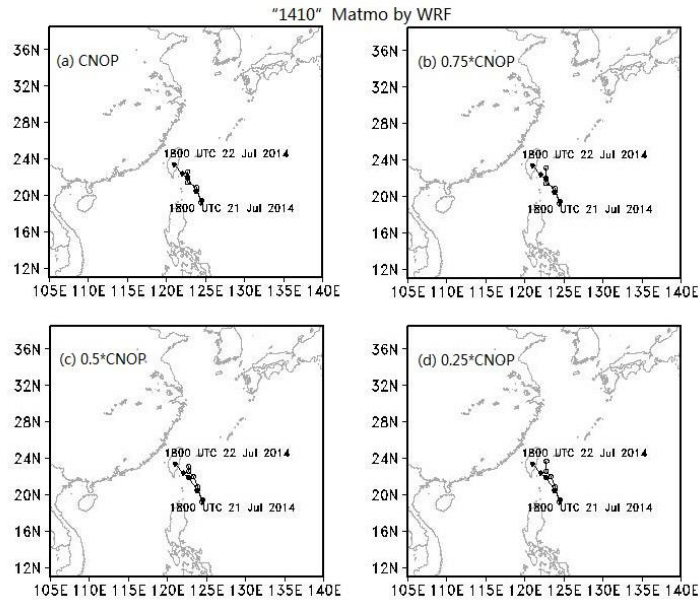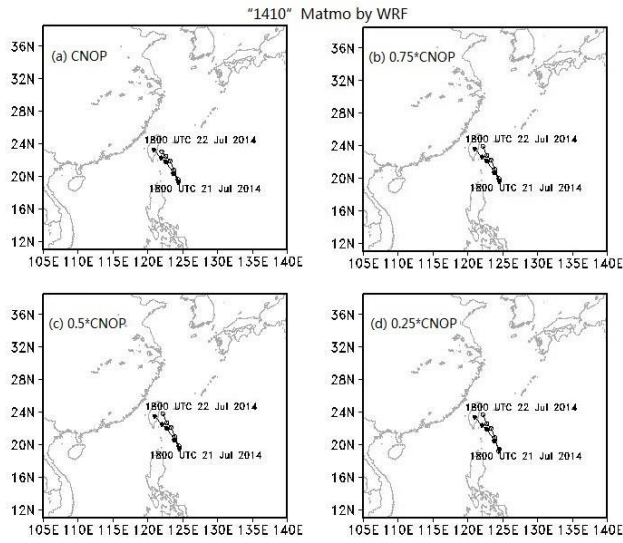
Figure 11: Simulated typhoon tracks of WRF-ARW with adding ACPW-CNOP or W×ACPW-CNOP into the initial state in the whole domain for Matmo. Solid circles represent observed tracks of CMA, and hollow circles show the simulated tracks of the WRF-ARW model. (a), (b), (c) and (d) denote CNOP, 0.75×CNOP, 0.5×CNOP and 0.25×CNOP, respectively.
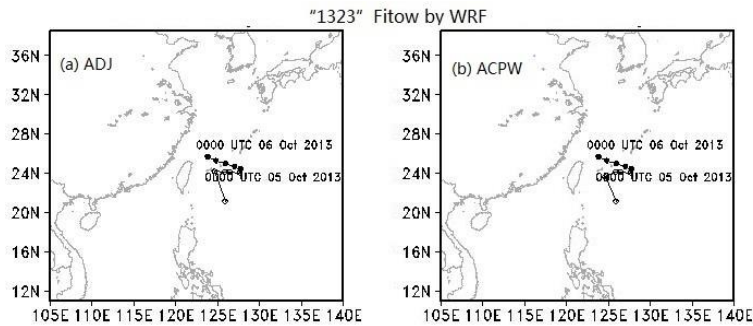
Figure 12: Simulated Fitow tracks of the WRF-ARW with adding modified CNOPs into the initial state. Solid circles represent observed typhoon tracks of CMA, and hollow circles show the simulated typhoon tracks of the WRF-ARW model. (a) is from ~~ADJ method~~ADJ method **and (b) is ACPW method.**
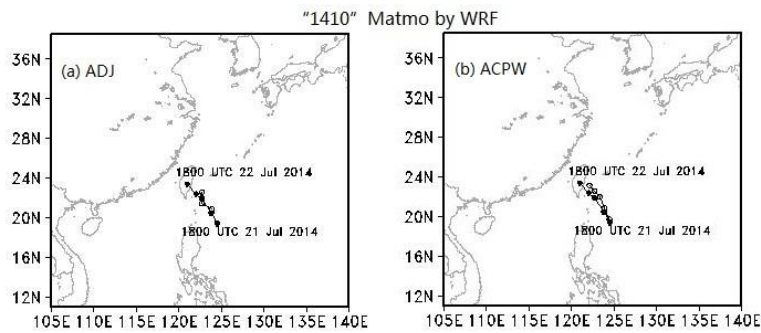
Figure 13: Simulated Matmo tracks of the WRF-ARW with adding modified CNOPs into the initial state. Solid circles represent observed typhoon tracks of CMA, and hollow circles show the simulated typhoon tracks of the WRF-ARW model. (a) is from ~~ADJ method~~ADJ method **and (b) is ACPW method.**

5

Table 1: The pseudocode of ACPW.

Algorithm. ACPW

Initialization:

1: Set the parameters of ACPW in Table 2.

ACPW:

2: Randomly generate an initial perturbation swarm $P_0 = \{X_1^{n'},\ X_2^{n'},\ \cdots, X_N^{n'}\}$, where $X^{n'} = \{x_1, x_{2,}\cdots, x_{n'}\}, x_i \in [-1,1], i = [1, n']$, and n' is the number of principal components selected;

3: According to the adaptive coefficient α, divide the entire initial swarm P_0 into two subswarms $P_0^1 = \{X_1^{n'},\ X_2^{n'},\ \cdots, X_{N\cdot\alpha}^{n'}\}$ and $P_0^2 = \{X_{N-N\cdot\alpha}^{n'},\ X_{N-N\cdot\alpha+1}^{n'},\ \cdots, X_N^{n'}\}$;

4: WHILE $t < Total\_Step$ DO;

5: $Project(X_t^{n'}, \zeta)$；Pull back the individual when it goes beyond the boundary, i.e., when $\|x_i\| > \zeta$, then $x_i = \frac{\zeta}{\|x_i\|} \times x_i$, ζ is the constrain condition in the formula (1);

6: $AdaptFun(P_i)$；Calculate the adaptive value of the objective function parallelly, i.e., $J(x_i)$ in Eq. (1).

7: Compare the values of the objective function of all individuals and save the best one;

8: ——Calculate the difference of the best objective function values of generations P_t and P_{t-1},

If the difference is smaller than the threshold value ε, then

change the adaptive coefficient α to $\alpha + 0.05$,

Else

change the adaptive coefficient α to $\alpha - 0.05$,

End if

9: Calculate the number of two subswarms by the new adaptive coefficient α;

10: Update the individuals of P_t^1 as the PSO rules;

11: Update the individuals of P_t^2 as the WSA rules;

12: END WHILE

Output: CNOP

Table 2: The control parameters of ACPW.

Name	Meaning	Value

n'	Number of principle components	in Table 6
N	Number of individuals	in Table 6
a	Adaptive coefficient	Initial: 0.5
ω	Inertia coefficient	0.8
$c1$	Self-awareness to track the historically optimal position	2.05
$c2$	Social-awareness of the particle swarm to track the globally optimal position	2.05
Υ	Restraint factor to control the speed	0.729
θ	Velocity of individual moving	0.5
r	Local optimizing radius	$8\times\delta$/original dimensions
s	Step size of updating individual	0.6
p_a	Probability of individual escaping from current position	0.3
$Total\_Step$	The number of iterations	in Table 6

Table 3: The meanings of all symbols

Symbols	Values/ components	Meanings
$\zeta\varphi_0$	$u'_0, v'_0, T'_0, p'_{s0},$	Initial perturbation
φ_{NT}	$u'_t, v'_t, T'_t, p'_{st}$	Nonlinear evolution of perturbed Φ_0 at time t
D	Values rely on cases	Verification area
η	(0, 1]	Vertical coordinate
c_p	1005.7 J kg−1 K−1	Specific heat at constant pressure
R_a	287.04 J kg−1K−1	Gas constant of dry air
T_r	270K	Constant parameter
p_r	1000hPa	Constant parameter

Table: 4 The numerical similarity between ACPW-CNOP and ADJ-CNOP

ACPW&ADJ	similarity
Fitow	0.61
Matmo	0.53

Table 5: Benefits (percent, %) achieved by reducing CNOPs in the sensitive regions.

Case	Method	0.75	0.5	0.25
Fitow	ADJ	6.9169%	6.9699%	6.669%

	ACPW	**10.2871%**	**9.6823%**	**8.812%**
Matmo	ADJ	0.0809%	0.083%	0.0779%
	ACPW	**2.3484%**	**3.5716%**	**5.2212%**

Table 6: the ~~running time~~time consumption **of ACPW for solving CNOP in the WRF-ARW model.**

n'	N	*Total_Step*	Time (units: minutes)	The adaptive value of objective function
30	20	10	89.83	28126.185933
30	40	10	179.55	27125.406996
30	60	10	269.33	26708.582565
30	40	20	359.79	30421.490441
40	30	10	136.77	24525.656206
40	40	20	360.43	31055.582842
50	30	10	136.89	17137.857070
60	30	10	137.23	14285.603508

Table 7: The Fitow tracks of adding different CNOPs with the WRF-ARW model. The red number represents the different position at the same time point.

Method/Fitow (2013)	Time	CNOP	0.75CNOP	0.5CNOP	0.25CNOP	0.5Sens
ADJ	0000 UTC 5 Oct	127.618 23.5222	127.652 24.0799	127.652 24.0799	127.652 24.0799	127.652 24.0799
	0600 UTC 5 Oct	126.43 24.1385	126.43 24.1385	126.43 24.1385	126.43 24.1385	126.43 24.1385
	1200 UTC 5 Oct	125.207 24.187	125.819 24.1641	125.819 24.1641	125.819 24.1641	125.819 24.1641
	1800 UTC 5 Oct	124.574 23.6492	124.574 23.6492	124.574 23.6492	124.595 24.2075	124.595 24.2075
	0000 UTC 6 Oct	125.874 21.1697	125.874 21.1697	125.874 21.1697	125.874 21.1697	125.874 21.1697
ACPW	0000 UTC 5 Oct	127.652 24.0799	127.652 24.0799	127.652 24.0799	127.652 24.0799	127.652 24.0799
	0600 UTC 5 Oct	126.43 24.1385	126.43 24.1385	126.43 24.1385	126.43 24.1385	126.43 24.1385
	1200 UTC 5	125.819	125.819	125.819	125.819	125.819

	Oct	24.1641	24.1641	24.1641	24.1641	24.1641
	1800 UTC 5	124.595	124.595	124.595	124.595	124.574
	Oct	24.2075	24.2075	24.2075	24.2075	23.6492
	0000 UTC 6	125.874	125.874	125.874	125.874	125.874
	Oct	21.1697	21.1697	21.1697	21.1697	21.1697

Table 8: The Matmo tracks of adding different ADJ-CNOPs with the WRF-ARW model. The red number represents the different position at the same time point.

Method/Matmo (2014)	Time	CNOP	0.75CNOP	0.5CNOP	0.25CNOP	0.5Sens
ADJ	1800 UTC	124.413	124.413	124.413	124.413	124.413
	21 Jul	19.193	19.193	19.193	19.193	19.193
	0000 UTC	123.876	123.876	123.876	123.876	123.876
	22 Jul	20.8786	20.8786	20.8786	20.8786	20.8786
	0600 UTC	122.696	122.696	123.31	123.31	122.696
	22 Jul	21.4631	21.4631	22.0081	22.0081	21.4631
	1200 UTC	122.708	122.708	122.72	122.72	122.708
	22 Jul	22.0207	22.0207	22.5785	22.5785	22.0207
	1800 UTC	122.72	122.733	122.733	122.745	122.72
	22 Jul	22.5785	23.1367	23.13	23.695	22.5785
ACPW	1800 UTC	124.433	124.433	124.433	124.413	124.433
	21 Jul	19.7486	19.7486	19.7486	19.193	19.7486
	0000 UTC	123.876	123.876	123.876	123.876	123.876
	22 Jul	20.8786	20.8786	20.8786	20.8786	20.8786
	0600 UTC	123.31	123.31	123.31	123.31	123.31
	22 Jul	22.0081	22.0081	22.0081	22.0081	22.0081
	1200 UTC	122.72	122.72	122.72	122.72	122.72
	22 Jul	22.5785	22.5785	22.5785	22.5785	22.5785
	1800 UTC	122.125	122.135	122.135	122.135	122.125
	22 Jul	23.1468	23.7051	23.7051	23.7051	23.1468